

# Evaluation of a Tight Frame Reconstruction Algorithm for Perfusion C-arm CT Using a Realistic Dynamic Brain Phantom

Michael Manhart<sup>\*†</sup>, Andreas Fieselmann<sup>\*†</sup> and Yu Deuerling-Zheng<sup>†</sup>

**Abstract**—This work introduces and evaluates an iterative, compressed sensing (CS) reconstruction algorithm based on tight frame regularization for perfusion C-arm CT with a high C-arm rotation speed acquisition protocol. To allow a realistic evaluation, a digital 4D brain phantom was created by extending a recently published phantom emulating time attenuation curves (TACs) inside a virtual brain segmented from clinical MR data. We additionally incorporated MR data to vary perfusion parameters all over the brain to avoid unrealistic homogeneous structures favoring CS algorithms. The iterative algorithm is compared to the Feldkamp algorithm by evaluating the root mean square error of the reconstructed TACs and Pearson correlation of the reconstructed perfusion maps to the ground truth. The results indicate that the tight frame algorithm qualitatively and quantitatively improves reconstructed perfusion maps compared to the Feldkamp algorithm.

## I. INTRODUCTION

Perfusion CT (PCT) is an important imaging modality for diagnosis in case of an ischemic stroke event. Time attenuation curves (TACs) in tissue and vessels are extracted from a time series of brain volumes acquired after a contrast bolus injection. Perfusion parameter maps calculated from TACs, such as cerebral blood flow (CBF), cerebral blood volume (CBV), and mean transit time (MTT), provide information about the extent of the affected tissue. They can be used to identify potentially salvageable ischemic tissue that could be reperfused by catheter-guided stroke therapy procedures such as intra-arterial thrombolysis. For this purpose the patient is transported to an interventional suite with C-arm angiography systems, where perfusion measurement is not yet available. Perfusion measurement using C-arm systems would allow assessing the perfusion parameters directly before and during the interventional procedure and help to determine the treatment success and endpoint. Yet the low rotation speed of common C-arm systems, which typically need  $\sim 5$  s to acquire one volume, makes perfusion C-arm CT (PCCT) challenging. Future C-arm systems with an increased rotation speed of up to  $100^\circ/\text{s}$  (Artis zeego, Siemens AG, Forchheim, Germany) will enable protocols with reduced acquisition time. In this study a potential protocol with fast C-arm rotation speed is simulated. The protocol consists of two acquisition sequences: the first sequence acquires one sweep in forward and one in backward rotation direction before bolus injection to reconstruct

baseline volumes with static anatomical structures. The second sequence acquires seven consecutive sweeps with alternating forward and backward rotation direction after bolus injection. Each sweep acquires 133 projections in a  $200^\circ$  angular range and requires  $T_r = 2.8$  s for data acquisition with a pause of  $T_w = 1.2$  s between sweeps. Thus TACs can be sampled with a temporal resolution of  $T_s = T_r + T_w = 4$  s. However, using the well-known FDK algorithm [1] for reconstruction of the acquired volumes, the limited number of 133 projections leads to streak artifacts. Furthermore, the peaks of the tissue TACs typically lie in a range of  $\sim 5 - 10$  HU, thus perfusion imaging is very sensitive to noise. An important challenge is to find algorithms capable of reliably reconstructing tissue TACs at a higher noise level to limit the radiation exposure to the patient. Recently, new iterative reconstruction techniques have been proposed with a promising application to these challenges: exploiting the idea of CS that the volumes have a sparse representation under a certain transformation. A well-known example for such a transformation is the total variation (TV) norm which is applied by the ASD-POCS [2] and iTV [3] algorithms. In the context of perfusion imaging the TV norm was proposed in combination with a prior image in the PICCS [4], and additionally with a non-convex extension of the TV norm in the NCPICCS algorithm [5]. Another example for a transformation is the tight frame (TF) wavelet based approach presented in [6]. Also special model-based iterative [7] and analytical [8] algorithms have been proposed for reconstruction of dynamic projection data from slowly rotating acquisition systems by using temporal basis functions to approximate the TACs. The scope of this work is the realistic evaluation of an iterative algorithm using a modified version of the TF regularization suggested by Jia et al. [6] with an extension of the realistic digital brain perfusion phantom by Riordan et al. [9]. As discussed in [6] the TF approach has been found to have higher computational efficiency and maintains image contrast better than TV minimization, which are important features in interventional perfusion imaging. The brain phantom data and tools are published online to improve the reproducibility of this and future studies [10].

## II. MATERIALS AND METHODS

### A. Reconstruction Algorithms

1) *TF Shrink*: The iterative CS algorithm applies the GPU-based Algebraic Reconstruction Technique with Ordered Subsets (OS-ART) presented in [11] to ensure data consistency

<sup>\*</sup>Pattern Recognition Lab, FAU Erlangen-Nürnberg, Germany

<sup>†</sup>Siemens AG, Angiography & Interventional X-Ray Systems, Forchheim, Germany

Email: michael.manhart@cs.fau.de

between the measured projection data  $p$  and the reconstructed volume  $f(\mathbf{x}) : \mathbb{N}^3 \rightarrow \mathbb{R}$  with respect to the acquisition system matrix  $A$ . The projections are partitioned into 10 disjoint sets, the relaxation factor is initialized with  $\beta = 0.8$  and reduced by multiplication with  $\beta_r = 0.95$  after each iteration. After processing one subset of projections, all negative values in  $f$  are set to zero to obtain a physically correct solution. To reduce noise the wavelet based tight frame regularization proposed by Jia et al. [6] is used. The volume  $f$  is decomposed into 27 wavelet coefficients  $\alpha_i(\mathbf{x}) = \Psi_i(\mathbf{x}) \otimes f(\mathbf{x}), i = 0 \dots 26$  by convolving the volume with the discrete version of a redundant, piecewise linear 3D TF basis [12] consisting of a low-pass filter  $\Psi_0(\mathbf{x})$  and high-pass filters  $\Psi_i(\mathbf{x}), i = 1 \dots 26$ . For simplifying notation, we denote this decomposition by  $\alpha(\mathbf{x}) = Df(\mathbf{x})$ . Then a vector-shrinkage operation is applied to the coefficients, where the  $l_2$  norm of the high-pass coefficients  $\tau_h(\mathbf{x}) = \sqrt{\sum_{i=1}^{26} \alpha_i(\mathbf{x})^2}$  determines whether the high-pass coefficients are kept or discarded. The shrinkage parameter  $\mu$  controls the level of suppressing the high-pass coefficients. In practice the regularization has shown to smoothen out the high contrast vessels, which can lead to underestimation of the contrast attenuation inside the vessels and blurring of the vessel into the encircling tissue. Thus, the shrinkage step is modified by excluding voxels containing vessel structures from the regularization. A vessel mask  $V(\mathbf{x}) : \mathbb{N}^3 \rightarrow \{0, 1\}$  was created by simple thresholding a baseline subtracted FDK reconstruction of a sweep with high contrast attenuation. The vector-shrinkage operator  $\mathcal{T}_\mu^V$  is then defined as:

$$\mathcal{T}_\mu^V \alpha_i(\mathbf{x}) = \begin{cases} \alpha_i(\mathbf{x}) & i = 0 \text{ or } V(\mathbf{x}) = 1, \\ \alpha_i(\mathbf{x}) \max \left[ \frac{\tau_h(\mathbf{x}) - \mu}{\tau_h(\mathbf{x})}, 0 \right] & \text{otherwise.} \end{cases} \quad (1)$$

After the shrinkage step the volume is recomposed from the new coefficients  $f(\mathbf{x}) = \sum_{i=0}^{26} \Psi_i(-\mathbf{x})\alpha_i(\mathbf{x})$ , for simplicity denoted by  $f(\mathbf{x}) = D^T \alpha(\mathbf{x})$ . The iterations stop when data consistency has not improved after one full iteration.

---

#### Algorithm 1 TF Shrink

---

- 1) Initialize:  $f^0 = 0, \epsilon^0 = \|Af^0 - p\|_2, k = 0$
  - 2) Do
  - 3)      $f^{output} = f^k, k = k + 1$
  - 4)      $f^k = \text{OS-ART}(f^{k-1})$  (3 Iterations)
  - 5)     Shrinkage:  $f^k = D^T \mathcal{T}_\mu^V D f^k$
  - 6)      $\epsilon^k = \|Af^k - p\|_2$
  - 7) While ( $\epsilon^k < \epsilon^{k-1}$ )
- 

2) *FDK*: The iterative algorithm is compared to standard FDK reconstruction with Parker short-scan weights [13]. The filtering step uses a Shepp-Logan filter kernel multiplied with a Gaussian of variance  $\sigma^2$  controlling smoothness and noise level in the reconstructed volumes.

#### B. Realistic Dynamic Brain Phantom

Classical digital CT phantoms usually consist of homogeneous structures and have a very sparse representation in TV or

wavelet transformation. This highly favors CS reconstruction algorithms, which exploit sparse representations. Thus, simple extensions to 4D dynamic phantoms do not allow for an authentic evaluation. We adopted the dynamic head phantom from [9], which was originally used for evaluation of perfusion parameter calculation methods, to create an appropriate phantom for evaluating the reconstruction algorithms. Similarly to what is proposed in [9], we segmented brain MRI scans from a human volunteer into white and gray matter, cerebrospinal fluid (CSF), and arteries. White/gray matter and CSF segmentation was done from T1 weighted MRI data using the Freesurfer software [14]. Arteries were segmented from a time-of-flight acquisition by thresholding and manual post-processing. The segmentations were combined into a volume consisting of 150 slices with 256x256 voxels of isotropic size 1 mm<sup>3</sup>. Inside the volume two different tissue classes were annotated using ellipsoid ROIs: tissue with reduced CBF (2 ROIs, altogether 13197 mm<sup>3</sup>) and tissue with severely reduced CBF and CBV (2 ROIs, altogether 5761 mm<sup>3</sup>). Furthermore, a ROI of healthy tissue (87949 mm<sup>3</sup>) around the stroke affected areas was annotated for evaluation purposes. Figure 1a shows an example of an annotated brain slice. Tissue that was not annotated was simulated like healthy tissue. Different perfusion parameters were assigned to the annotated ROIs as shown in Table I. To further reduce the sparsity of the brain phantom, the MR data was used to vary the perfusion parameters. The parameters were varied according to the intervals shown in Table I. Details of this variation are provided at the phantom web page [10]. The tissue TACs were created as described in [9] by convolution of a real measured arterial input function (AIF) from clinical PCT with a residual function with exponential decay. For vessel structures the TACs were simulated by the real measured AIF. To incorporate the anatomic tissue structures into the phantom, appropriate constant HU values were added to the TACs like in [9]. Also, the HU values of the anatomic structures were varied using the MR data to reduce sparsity. Finally the dynamic C-arm projection data was created by forward projecting the 4D phantom according to the high C-arm rotation speed acquisition protocol. Poisson-distributed noise was added to the projections assuming an emitted X-ray density of  $2.1 \cdot 10^6$  photons per mm<sup>2</sup> at the source-to-detector distance as in [7].

#### C. Perfusion Parameter Calculation and Comparison

To compute perfusion parameters from the reconstructed data, the baseline volumes were subtracted from the dynamic volumes to extract the contrast attenuation. Then the TACs were created from the subtracted volumes. Each volume represents TAC samples at the mid time point of its acquisition. By linear interpolation the TACs were resampled to 1 s temporal resolution. A TAC inside the internal carotid artery was selected as AIF and the perfusion parameters were calculated using a deconvolution approach based on indicator-dilution theory [15]. For quantitative comparison of the reconstruction algorithms the root mean square error (RMSE) over time between the reconstructed and the ground truth time curves

of the AIF and inside the annotated tissue was computed. To compare the resulting perfusion maps the Pearson correlation (PC) between maps created from the reconstructed TACs and maps created from the ground truth TACs was computed. Two types of PC have been calculated: the first PC value takes only the annotated tissue into account. It is focused on the regions inside and close to the stroke affected tissue, stating how well it is separated from the healthy tissue. The second value represents all values of the stroke affected slices. This PC value incorporates the higher blurring of vessels in the perfusion maps of smoother reconstructions.

### III. RESULTS

Figure 1 shows the resulting CBF, CBV, and MTT perfusion maps from FDK reconstruction with  $\sigma = 1.25$  mm, TF Shrink reconstruction with  $\mu = 0.0001$ , and the reference images for comparison. Table II shows the quantitative results for different parameters, where the best result for each measure is shown in bold. The reconstructions were performed on a laptop computer with an Intel i7 M 620 2 x 2.7 GHz CPU, 8 GB RAM and an Nvidia Quadro FX 880M graphic chipset. The GPU-based implementation required  $\sim 50$  s for one complete TF Shrink iteration, the complete reconstruction of 9 volumes of size  $256 \times 256 \times 180$  varied between  $\sim 30 - 75$  min depending on the shrinkage parameter  $\mu$ . Complete reconstruction with FDK took  $\sim 1.5$  min.

### IV. DISCUSSION

The perfusion maps in Figure 1 show that the maps created from the TF Shrink reconstructions have a qualitatively good correspondence with the reference maps for CBF and CBV. Stroke affected areas are well separated from the healthy regions. In the TF Shrink MTT map the areas with reduced CBF are well visible. However, the areas with severely reduced CBF/CBV are not visible. Since  $MTT = \frac{CBV}{CBF}$  and both CBV and CBF values are very low in these regions, it is very challenging to estimate under noisy conditions. In the maps generated from the FDK reconstructions the affected regions are still visible in the CBF and CBV map but not as well separated from the healthy tissue as in the TF Shrink maps. The FDK MTT map does not allow for a reliable location of the stroke affected areas. This corresponds to the quantitative results in Table II. The TF Shrink algorithm has the best PC for most maps with  $\mu = 10^{-4}$ , e.g. the PC of the CBF map can be increased from 0.79 for the best FDK reconstruction to 0.86. The results also show the advantage of excluding the vessels from regularization, which reduces blurring of vessels and underestimation of contrast attenuation values in vessels. The RMSE of the AIF estimation is improved from 155 HU to 86 HU for  $\mu = 5 \cdot 10^{-4}$ .

### V. CONCLUSIONS

This work shows that iterative reconstruction with tight frame regularization has significant potential to improve perfusion C-arm CT with a fast acquisition protocol. Qualitative and quantitative comparisons of the reconstructed perfusion

maps were done using a realistic brain phantom that avoids the sparse structure of classical CT phantoms. Visual impression and correlation of the reconstructed maps to the ground truth is significantly improved compared to the FDK reconstruction results. However, computation time is increased compared to FDK reconstruction, which is critical in interventional applications. Nevertheless, further code optimization and the rapid development of hardware will likely make this approach clinically applicable in the foreseeable future.

### ACKNOWLEDGMENT

The authors thank Robert Grimm and Jana Hutter for help with the MR acquisitions for the brain phantom.

### REFERENCES

- [1] L. Feldkamp, L. Davis, and J. Kress, "Practical cone-beam algorithm," *Journal of the Optical Society of America A*, vol. 1, no. 6, pp. 612–619, 1984.
- [2] E. Y. Sidky and X. Pan, "Image reconstruction in circular cone-beam computed tomography by constrained, total-variation minimization," *Physics in Medicine and Biology*, vol. 53, no. 17, pp. 4777–4807, 2008.
- [3] L. Ritschl, F. Bergner, C. Fleischmann, and M. Kachelrieß, "Improved total variation-based CT image reconstruction applied to clinical data," *Physics in Medicine and Biology*, vol. 56, no. 6, pp. 1545–1561, 2011.
- [4] B. E. Nett, R. Brauweiler, W. Kalender, H. Rowley, and G.-H. Chen, "Perfusion measurements by micro-CT using Prior Image Constrained Compressed Sensing (PICCS): Initial Phantom Results," *Physics in Medicine and Biology*, vol. 55, no. 8, pp. 2333–2350, 2010.
- [5] J. C. Ramirez-Giraldo, J. Trzasko, S. Leng, L. Yu, A. Manduca, and C. McCollough, "Nonconvex prior image constrained compressed sensing (NCPICCS): Theory and simulations on perfusion CT," *Medical Physics*, vol. 38, no. 4, pp. 2157–2167, 2011.
- [6] X. Jia, B. Dong, Y. Lou, and S. B. Jiang, "GPU-based iterative cone-beam CT reconstruction using tight frame regularization," *Physics in Medicine and Biology*, vol. 56, no. 13, pp. 3787–3807, 2011.
- [7] C. Neukirchen, M. Giordano, and S. Wiesner, "An iterative method for tomographic x-ray perfusion estimation in a decomposition model-based approach," *Medical Physics*, vol. 37, no. 12, pp. 6125–6141, 2010.
- [8] C. Neukirchen, "An extended temporal interpolation approach for dynamic object reconstruction," in *Proceedings 11th Fully 3D*, 2011, pp. 379–382.
- [9] A. J. Riordan, M. Prokop, M. A. Viergever, J. W. Dankbaar, E. J. Smit, and H. W. A. M. de Jong, "Validation of CT brain perfusion methods using a realistic dynamic head phantom," *Medical Physics*, vol. 38, no. 6, pp. 3212–3221, 2011.
- [10] Digital Brain Perfusion Phantom. <http://www5.cs.fau.de/data/>.
- [11] B. Keck, H. Hofmann, H. Scherl, M. Kowarschik, and J. Hornegger, "GPU-Accelerated SART Reconstruction Using the CUDA Programming Environment," in *Proc. SPIE*, 2009.
- [12] B. Dong and Z. Shen, "MRA-based wavelet frames and applications," IAS Lecture Notes Series, Summer Program on "The Mathematics of Image Processing", Tech. Rep., 2010.
- [13] D. L. Parker, "Optimal short scan convolution reconstruction for fan beam CT," *Medical Physics*, vol. 9, no. 2, pp. 254–257, 1982.
- [14] Freesurfer image analysis suite. <http://surfer.nmr.mgh.harvard.edu/>.
- [15] A. Fieselmann, M. Kowarschik, A. Ganguly, J. Hornegger, and R. Fahrig, "Deconvolution-Based CT and MR Brain Perfusion Measurement: Theoretical Model Revisited and Practical Implementation Details," *International Journal of Biomedical Imaging*, 2011, article ID 467563.

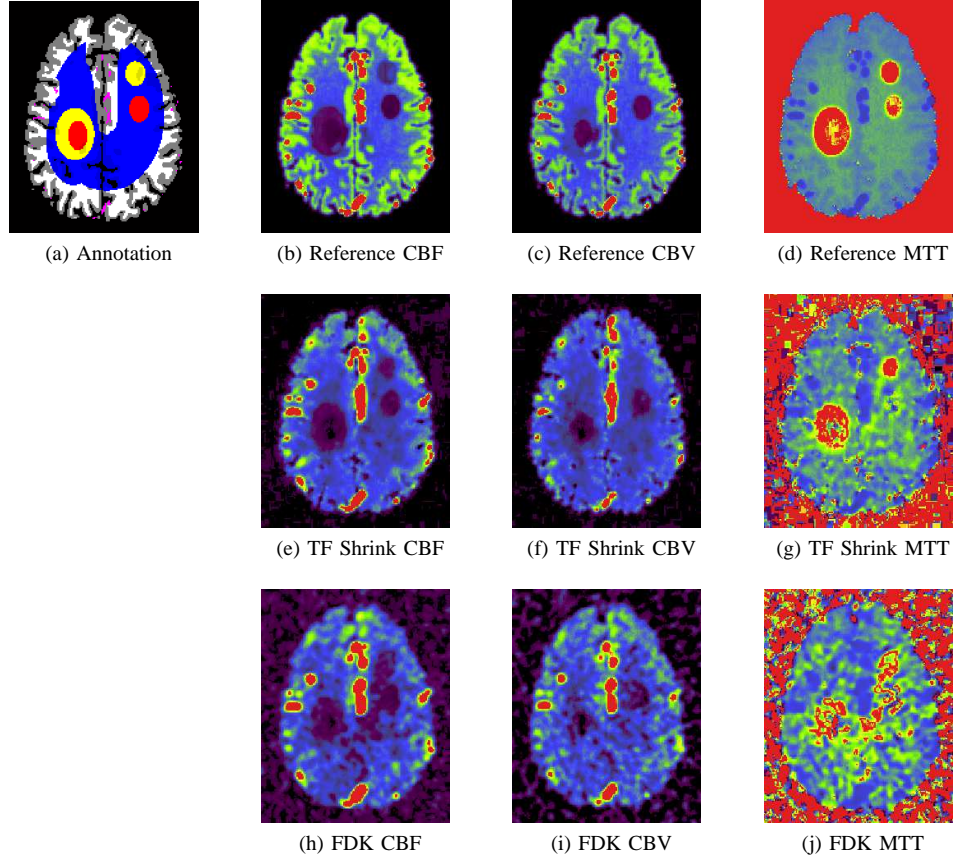


Fig. 1. Perfusion maps (Annotation legend: yellow: reduced CBF area, red: reduced CBF/CBV area, blue: healthy tissue area used for evaluation).

	Healthy		Reduced CBF		Reduced CBF/CBV	
	WM	GM	WM	GM	WM	GM
CBF [ml/100 ml/min]	$25 \pm 14$	$53 \pm 14$	$7.5 \pm 4.25$	$16 \pm 4.25$	$2.5 \pm 1.4$	$5.3 \pm 1.4$
CBV [ml/100 ml]	$1.9 \pm 0.9$	$3.3 \pm 0.4$	$1.7 \pm 0.9$	$3 \pm 0.7$	$0.42 \pm 0.2$	$0.71 \pm 0.12$
MTT [s]	$4.6 \pm 0.7$	$3.7 \pm 0.7$	$14 \pm 0.75$	$11 \pm 0.75$	$10 \pm 1$	$8 \pm 1$

TABLE I  
PERFUSION PARAMETERS (WM = WHITE MATTER, GM = GRAY MATTER).

Algorithm	FDK					Tight Frame Regularization			w.o. vessel mask
	$\sigma = 0.5$	0.75	1.0	1.25	1.5	$\mu = 5 \cdot 10^{-5}$	$1 \cdot 10^{-4}$	$5 \cdot 10^{-4}$	$5 \cdot 10^{-4}$
RMSE Tissue [HU]	7.26	4.27	3.08	2.54	2.29	2.52	2.21	<b>2.15</b>	2.20
RMSE AIF [HU]	78	119	156	184	204	<b>53</b>	58	86	155
PC CBF (annotated tissue)	0.68	0.75	0.78	0.79	0.78	0.84	<b>0.86</b>	0.84	0.80
PC CBV (annotated tissue)	0.54	0.62	0.68	0.71	0.72	0.77	<b>0.79</b>	0.77	0.76
PC MTT (annotated tissue)	0.35	0.47	0.58	0.66	0.73	<b>0.81</b>	<b>0.81</b>	0.80	0.80
PC CBF (complete tissue)	0.65	0.69	0.68	0.64	0.61	0.73	<b>0.76</b>	0.71	0.64
PC CBV (complete tissue)	0.52	0.59	0.62	0.61	0.59	0.67	<b>0.72</b>	0.69	0.64
PC MTT (complete tissue)	0.32	0.43	0.55	0.64	0.71	0.70	0.75	<b>0.78</b>	<b>0.78</b>
Iterations/Volume	N/A	N/A	N/A	N/A	N/A	4	6	10	4

TABLE II  
QUANTITATIVE RESULTS.